PERGAMON

International Journal of Solids and Structures 38 (2001) 1327–1339

INTERNATIONAL JOURNAL OF SOLIDS and STRUCTURES

www.elsevier.com/locate/ijsolstr

Analytic solutions for fundamental eigenfrequencies of optical actuators in six directions of motion

Yoon Young Kim *, Ho Cheol Lee

School of Mechanical and Aerospace Engineering, Institute of Advanced Machinery and Design, Kwanak-Gu Shinlim-Dong, San 56-1, Seoul 151-742, South Korea

Received 7 May 1999; in revised form 25 February 2000

Abstract

Perhaps, this is the first paper that derives analytic solutions for the fundamental eigenfrequencies in all six directions of motion in optical actuators. The specific analysis is conducted for actuators suspended by four cantilevered beams having rectangular bends near the beam ends. While some existing reports consider only one or two translational motions, the present paper considers all six motions including rotational motions. The well-known Castigliano theorem is employed for the prediction of stiffness in the six directions of motion. The use of simple, approximate deformed shapes for all directions is newly proposed in this work. The correct deformed shapes play a crucial role in the analysis. The validity of the present results is verified by comparison with finite element results. As a practical application of the present approach, an optimal suspension beam sizing problem is considered.

Keywords: Optical actuator; Eigenfrequency; Analytic solution

1. Introduction

In many optical actuators, the optimal structural design of actuators satisfying design specifications is very important. This is because the performance of the whole optical system such as access speed and stability greatly depends on the structural dynamics of the actuator. Similarly, the importance of the structural characteristics is also addressed in some sensors. For instance, a multi-axis acceleration vector sensor must have good dynamic characteristics in terms of resonant frequencies, bandwidth, etc. (Göpel et al., 1994).

Among the various sensors and actuators, the present work is mainly concerned with the analytic determination of the fundamental eigenfrequencies of an optical pickup in six directions of motion. Optical pickup systems become more important devices for large capacity storage (Zheng, 1994). The analytic solutions for the fundamental eigenfrequencies using a simplified model of an actuator can play an

* Corresponding author. Tel.: +82-2-880-7154; fax: +82-2-883-1513.
E-mail address: yykim@snu.ac.kr (Y.Y. Kim).

0020-7683/01/$ - see front matter
PII: S0020-7683(00)00054-8

important role in an early design step. Since early design optimization requires a considerable amount of calculations, the present simplified analysis allows easy design changes and gives an insight into the given design problems in comparison with finite element analysis.

Fig. 1 shows an optical pickup system used to retrieve the information recorded on an optical disk (see Bouwhuis et al. (1985) for the principle of optical disk systems). It mainly consists of an objective lens, a coil and a bobbin. The bobbin holding the objective lens is supported by four suspension beams.

In order to read correctly the information recorded on a disk using a laser beam, correct tracking and focusing of the laser beam is most important. Unfortunately, tracking and focusing motions cannot be completely free from unwanted motions such as the tilting motion. Therefore, designing an optical pickup system requires the understanding of the system dynamic characteristics of actuators not only for the tracking and focusing motions, but also for other motions including rotational motions. Subsequently, the fundamental eigenfrequencies and mode shapes in three translational and three rotational motions of a bobbin must be known. The present work is devoted to such analysis and derives analytic solutions for all of the six directions of motion for the first time.

The papers on the analysis of actuator dynamic characteristics are very limited. Kajiwara and Nagamatsu (1993) have introduced a structural design technique in order to handle problems related to resonance. In a recent study, Kim et al. (1999) have shown the usefulness of the rectangular bends in the suspension beams of an actuator and proposed a rigid-body structural model of the actuator. Lee et al. (1997) used a simpler model for the dynamic analysis of an actuator. However, these works are limited to the analytic determination of fundamental eigenfrequencies only in tracking and focusing the directions.

Considering the importance of fundamental eigenfrequencies in all directions of motion for the structural design of actuators, the analytic determination of all the six fundamental eigenfrequencies is extremely useful. This will facilitate the initial structural design of an actuator. The goal of this work is to present an analytic approach to calculate the fundamental eigenfrequencies of an actuator in all directions of motion. Although the bobbin tilting modes having high eigenfrequencies must be suppressed, the fundamental modes having low eigenfrequencies that are governed mainly by the suspension stiffness must be understood in order to select the optimal and cost-effective controllers.

To derive all the six fundamental eigenfrequencies, the actuator suspended by four cantilevered beams is modeled as a one-degree-of-freedom spring–mass system in each of the six directions of motion. Castigliano's theorem is adopted in order to derive the stiffness in each direction of motion. However, the crucial step in the present analysis is the correct prediction of deformed shapes of the suspension system, partic-

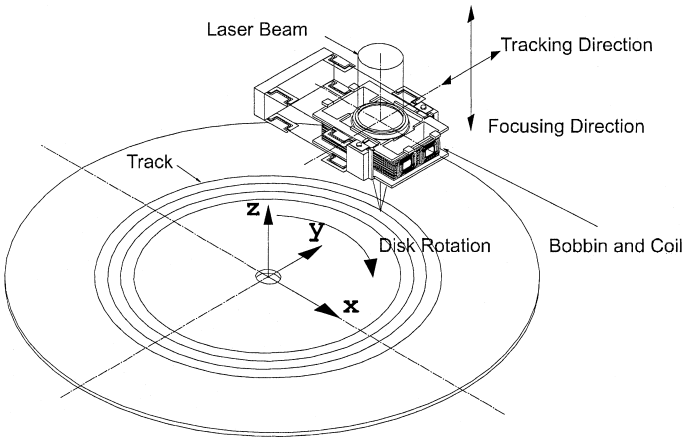

Fig. 1. Schematic figure of an optical actuator system.

ularly for the rotational motion. Furthermore, the imposition of approximate mode-orthogonality conditions is the most important procedure in the analysis of rotational modes; without the approximate conditions, the analysis would be impractically complicated. These issues are addressed in detail in the present work.

The validity of the present analysis is verified by comparing the present results with finite element results. To show the usefulness of the present approach, a suspension beam sizing optimization problem is considered. Although the present work is carried out for a specific optical pickup system, the present technique can be easily extended to deal with a wider class of actuator design problems.

2. Modeling

The optical actuator system in consideration has four suspension beams with rectangular bends at both the ends of each of the beam as shown in Fig. 1. The effectiveness of the use of the bends has been addressed earlier by Kim et al. (1999). For a low frequency range which is governed by the fundamental frequencies in six directions of motion, the assembly of a bobbin, a coil and an objective lens behaves as a rigid body (Kim et al., 1999). Subsequently, the optical system is modeled as a concentrated mass supported by four suspension beams; (see Fig. 2). The concentrated mass (mass: M_c, moments of inertia: I_x, I_y, I_z) can be assumed to be connected to suspension beams by four rigid links.

In investigating the fundamental frequencies in six directions of motion, the stiffness of the suspension beams in each direction of motion of interest needs to be evaluated. Once the stiffness of the assembly of four suspension beams is known, the fundamental frequencies are easily found from the following simple equation:

$$\omega = \sqrt{\frac{\text{stiffness}}{\text{mass}}} = \sqrt{\frac{k_i}{m_i}}, \tag{1}$$

where mass (m_i) and stiffness (k_i) should be understood as the inertia and rotational stiffness when rotational motions are considered. (The use of Eq. (1) can be justified since the magnitude of the concentrated mass is much larger than that of the suspension beam mass.) Therefore, the present problem can be reduced to a problem of determining the suspension beam stiffness.

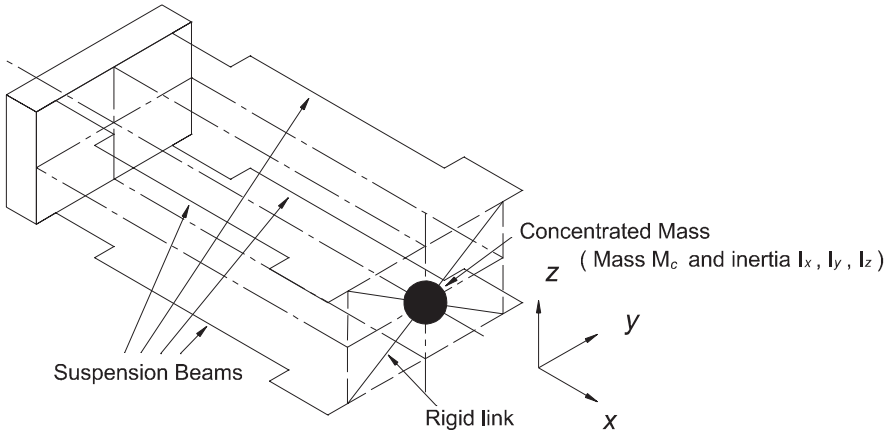

Fig. 2. Proposed modeling of an optical actuator and suspension beams.

Though the evaluation of the suspension beam stiffness in the translation directions of x and y is rather straightforward, the stiffness in the other directions of motion is not. Rotational stiffness, in particular, requires careful considerations of deformed shapes of beams as well as the distance between the concentrated mass and the tips of the suspension beams. In addition, kinematic compatibilities between the concentrated mass and the suspension beams need to be carefully considered. A detailed analysis is given in Section 3.

3. Evaluation of suspension beam stiffness

In determining the suspension beam stiffness, it should be noted that when an external force (or moment) is applied at the concentrated mass (point A in Fig. 3), not only the force in the direction of the external force, but also forces (and moments) in other directions are produced inside the suspension beams. Therefore, for each of the three forces and three moments applied at the concentrated mass (denoted by F_i^{ext} and M_i^{ext}, $i = x, y, z$), we must consider the forces and moments acting on the tip of each of the suspension beams (denoted by F_i^{int} and M_i^{int}, $i = x, y, z$). The subscripts i in F_i and M_i denote the direction of the force (or moment). Using the symmetry of the suspension beams, it will be sufficient to consider the deformation of one of the four beams. As indicated in Fig. 3, the suspension beams have rectangular cross-sections with varying thickness (t) and width (b). Although a typical etching process produces uniform beam thickness (t), the thickness is assumed to vary.

Since each beam segment has larger orders of axial stiffness in comparison to stiffness in other directions, we ignore the contribution of the axial stretch to the beam complementary energy. If three forces $(F_x^{\text{ext}}, F_y^{\text{ext}}, F_z^{\text{ext}})$ and three moments $(M_x^{\text{ext}}, M_y^{\text{ext}}, M_z^{\text{ext}})$ are assumed to be applied at the tip, the stored complementary energy U is

$$U = U_{\text{AB}} + U_{\text{BC}} + U_{\text{CD}} + U_{\text{DE}} + U_{\text{EF}} + U_{\text{FG}} + U_{\text{GH}}. \tag{2}$$

The expressions for U_{AB}, etc. are listed in Appendix A.

As may be evident in the formula given in Appendix A, the complementary energies associated with two bending deformations and a twisting deformation are taken into account. In Section 4, we present a technique to impose correct tip conditions. These conditions represent kinematic compatibilities, equilibrium and approximate mode-orthogonality conditions.

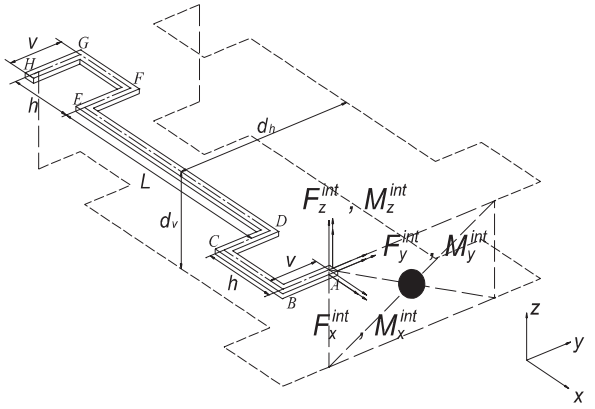

Fig. 3. Detailed geometry of a suspension beam. Forces and moments that can be developed at the tip (tip A) of the beam are also shown.

Now, we present a procedure to determine the stiffness of the assembly of the four suspension beams when external forces (or moments) are applied at the concentrated mass. We begin with the analysis of translational stiffness, which is relatively easy except for the translational stiffness in the x direction. Then, we present the analysis for the rotational stiffness.

3.1. Translational stiffness k_x^{tr} in the x direction

Fig. 4 describes the deformed shape of the suspension system when an external force F_x^{ext} is applied. Under F_x^{ext}, only the following tip force and moment components are nonvanishing:

$$F_x^{\text{int}} \neq 0, \quad M_y^{\text{int}} \neq 0, \quad M_z^{\text{int}} \neq 0.$$

The consideration of the force equilibrium in the x direction determines the magnitude of the force F_x^{int} at the tip of each beam as

$$F_x^{\text{int}} = \frac{F_x^{\text{ext}}}{4}. \tag{3}$$

Now, we consider the kinematic compatibilities. Since the tip of the beam is rigidly attached to the concentrated mass (i.e. the bobbin assembly), the tip rotation θ_z about the z axis must vanish. Similarly the tip displacement δ_y in the y direction must vanish; the beam is rigidly connected to the mass and the suspension beam has symmetry about the xz plane. Therefore, a force F_y^{int} and a moment M_y^{int} are developed at the tip, which can be determined by applying Castigliano's theorem (Washizu, 1982):

$$\theta_z = \frac{\partial U}{\partial M_z^{\text{int}}} = 0, \qquad \delta_y = \frac{\partial U}{\partial F_y^{\text{int}}} = 0. \tag{4}$$

Since the beam displacement is equal to the displacement (δ_x) of the concentrated mass, the following equation can be used:

$$\frac{\partial U}{\partial F_x^{\text{int}}} = \delta_x. \tag{5}$$

By solving Eqs. (3)–(5) simultaneously, the stiffness, k_x^{tr}, of the beam assembly can be found:

$$k_x^{\text{tr}}(h, v, L, b, t, d_w, d_h, t_{\text{AB}}, t_{\text{BC}}, \ldots, t_{\text{GH}}, b_{\text{AB}}, b_{\text{BC}}, \ldots, b_{\text{GH}}) = \frac{F_x^{\text{ext}}}{\delta_x}. \tag{6}$$

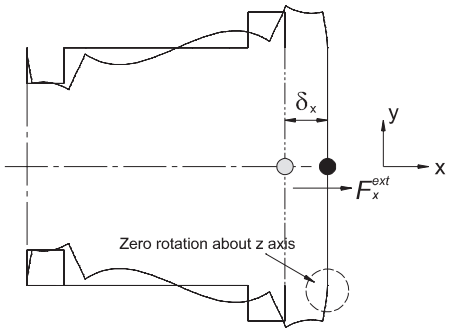

Fig. 4. Deformed shape under F_x^{ext}.

In Eq. (6), the superscript tr stands for 'translation.' The thickness and width of the segment ij of the beam are denoted by t_{ij} and b_{ij}, respectively. Although the explicit expression of k_x^{tr} in Eq. (6) is not written out here, Eq. (6) indicates that there are considerably many variables that affect the beam stiffness. Part of these variables can be used as design variables and an optimization problem will be considered later.

3.2. Translational stiffness k_y^{tr} in the y direction

The predicted deformed shape of the optical actuator system subjected to F_y^{ext} is shown in Fig. 5. The nonvanishing components developed at the tip of each of the beams can be shown as

$$F_x^{\mathrm{int}} \neq 0, \qquad F_y^{\mathrm{int}} \neq 0, \qquad M_z^{\mathrm{int}} \neq 0.$$

Considering the equilibrium between F_y^{ext} and $(F_x^{\mathrm{int}}, F_y^{\mathrm{int}}, M_z^{\mathrm{int}})$, one can obtain the following results:

$$F_y^{\mathrm{ext}} = 4F_y^{\mathrm{int}}, \tag{7}$$

$$M_z^{\mathrm{int}} = -\frac{d_h}{2} F_x^{\mathrm{int}}. \tag{8}$$

Note that Eq. (8) states the moment equilibrium about the z axis.

A special care must be taken in considering the geometric compatibility. Obviously the applied force F_y^{ext} produces the displacement in the y direction, but it also causes the rotation θ_z of the suspension system as well as the tip displacement δ_x^{t} of each beam in the x direction (Fig. 5). With a small displacement assumption, the compatibility relation between δ_x^{t} and θ_z can be written as

$$\frac{d_h}{2}\theta_z = \delta_x^{\mathrm{t}}. \tag{9}$$

Now applying Castigliano's theorem with respect to $F_x^{\mathrm{int}}, F_y^{\mathrm{int}}$ and M_z^{int} yields

$$\frac{\partial U}{\partial F_y^{\mathrm{int}}} = \delta_y, \qquad \frac{\partial U}{\partial F_x^{\mathrm{int}}} = \delta_x^{\mathrm{t}}, \qquad \frac{\partial U}{\partial M_z^{\mathrm{int}}} = \theta_z^{\mathrm{t}}. \tag{10}$$

The solution of Eqs. (7)–(10) gives a closed-form expression for the stiffness k_y^{tr}:

$$k_y^{\mathrm{tr}} = \frac{F_y^{\mathrm{ext}}}{\delta_y}. \tag{11}$$

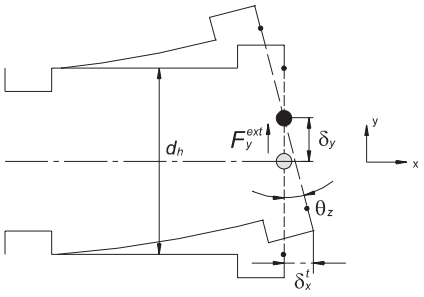

Fig. 5. Deformed shape under F_y^{ext}.

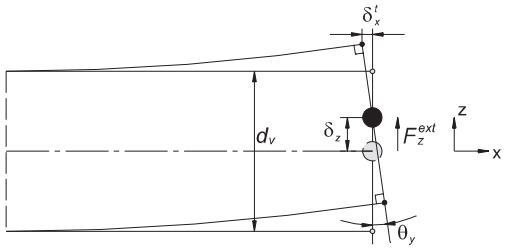

Fig. 6. Deformed shape under F_z^{ext}.

3.3. Translational stiffness k_z^{tr} in the z direction

The suspension deformation in the xz plane due to the force F_z^{ext} is described in Fig. 6. Due to the nonvanishing tip displacement δ_x^{t}, the suspension deformation in the xy plane looks like the one shown in Fig. 4(a). All the tip forces and moments must be considered in this case, and it is important to use the following condition:

$$\frac{d_v}{2}\theta_y = \delta_x^{\text{t}}, \tag{12}$$

$$F_z^{\text{ext}} = 4F_z^{\text{int}}, \tag{13}$$

$$M_y^{\text{int}} = -\frac{d_h}{2}F_x^{\text{int}}, \tag{14}$$

$$\frac{\partial U}{\partial F_z^{\text{int}}} = \delta_z, \qquad \frac{\partial U}{\partial F_x^{\text{int}}} = \delta_x^{\text{t}}, \qquad \frac{\partial U}{\partial M_y^{\text{int}}} = \theta_y, \qquad \frac{\partial U}{\partial M_x^{\text{int}}} = 0. \tag{15}$$

Examining the deformation in the xy plane and using the same approach used for k_x^{tr}, one can find k_z^{tr} using

$$\frac{\partial U}{\partial F_y^{\text{int}}} = 0, \qquad \frac{\partial U}{\partial M_z^{\text{int}}} = 0. \tag{16}$$

3.4. Rotational stiffness k_x^{rot} about the x axis

A special care must be taken in imposing the kinematic compatibility in this case. Fig. 7 describes the deformed shape of the actuator model viewed from the positive x axis. The rotation θ_x caused by the applied moment M_x^{ext} is accompanied by the tip displacements δ_y^{t} and δ_z^{t}. For a small rotation θ_x, the resulting δ_y^{t} and δ_z^{t} can be approximated as

$$\delta_y^{\text{t}} = r[\cos(\alpha) - \cos(\alpha + \theta_x)] \simeq r \sin\theta_x \sin\alpha \simeq r\theta_x \sin\alpha, \tag{17a}$$

$$\delta_z^{\text{t}} = r[\sin(\theta_x + \alpha) - \sin\alpha] \simeq r \sin\theta_x \cos\alpha \simeq r\theta_x \cos\alpha, \tag{17b}$$

where

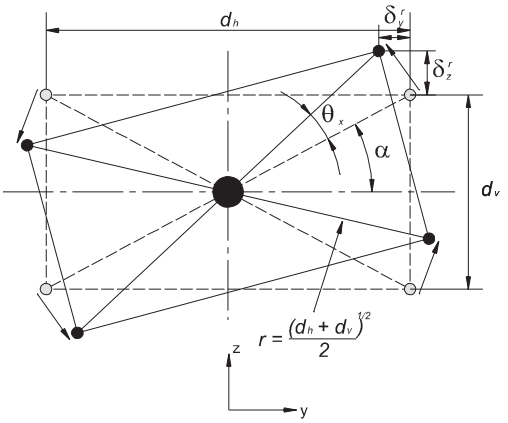

Fig. 7. Deformed shape under M_x^{ext}.

$$r = \frac{1}{2}(d_h + d_v)^{1/2}, \qquad \tan\alpha = \frac{d_v}{d_h}. \tag{18}$$

One can see that the nonvanishing tip force and moment components are $F_x^{\text{int}}, F_y^{\text{int}}$ and M_z^{int} when M_x^{ext} is applied at the concentrated mass. The moment equilibrium about the x axis is used to obtain the relation between M_x^{ext} and $(F_y^{\text{int}}, F_z^{\text{int}}, M_x^{\text{int}})$:

$$M_x^{\text{ext}} = 4F_z^{\text{int}}\frac{d_v}{2} + 4F_y^{\text{int}}\frac{d_h}{2} + 4M_x^{\text{int}}. \tag{19}$$

Other kinematic constraints provided by Castigliano's theorem are

$$\frac{\partial U}{\partial F_y^{\text{int}}} = \delta_y^{\text{t}}, \qquad \frac{\partial U}{\partial F_z^{\text{int}}} = \delta_z^{\text{t}}, \qquad \frac{\partial U}{\partial M_x^{\text{int}}} = \theta_x, \qquad \frac{\partial U}{\partial M_z^{\text{int}}} = 0. \tag{20}$$

Combining the equations above yields

$$k_x^{\text{rot}} = \frac{M_x^{\text{ext}}}{\theta_x}. \tag{21}$$

3.5. Rotational stiffness k_y^{rot} about the y axis

The predicted deformation shape of the suspension beam when the moment M_y^{ext} is applied at the concentrated mass is shown in Fig. 9. It is crucial to use the deformation shape depicted in Fig. 8(a), not in Fig. 8(b) for the rotational stiffness evaluation of the suspension beam. This is because we need the rotational stiffness that will be used for the prediction of the fundamental rotational frequency, not for the static response prediction. Fig. 8(b) shows the static deformation of the suspension beams under M_y^{ext}, but this deformation is similar to the deformation shown in Fig. 6. As a result, we propose to impose the following condition in order to select the deformed shape shown in Fig. 8(a):

$$\delta_z^{\text{tip}} = 0. \tag{22}$$

Note that the constraint expressed by Eq. (22) is an approximate mode-orthogonality condition between the fundamental translational mode in the z axis and the fundamental rotational mode in the y axis. This

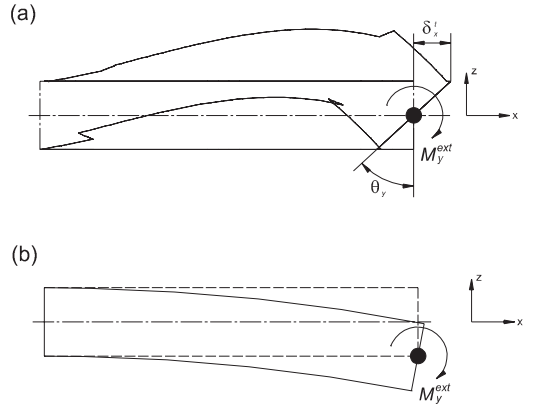

Fig. 8. (a) Correct and (b) incorrect deformed shapes under M_y^{ext} (the incorrect deformed shape is not orthogonal to the deformed shape under F_z^{ext}).

approximate orthogonality is crucial in selecting the correct mode shape. For the deformed shape in consideration, all the tip force and moment components except M_x^{int} are needed for the analysis.

Considering the moment equilibrium about the y axis, the following relation can be found:

$$M_y^{\text{ext}} = 4F_x^{\text{int}}\frac{d_h}{2} + 4M_y^{\text{int}}. \tag{23}$$

It is also important to note that the moment applied to the bobbin induces not only the corresponding rotation θ_y about the y axis, but also the translation δ_x^{t} in the x direction of the tips of the suspension beams.

The application of Castigliano's theorem yields, with the consideration of the discussions given above,

$$\frac{\partial U}{\partial F_x^{\text{int}}} = \delta_x^{\text{t}}, \qquad \frac{\partial U}{\partial F_y^{\text{int}}} = 0, \qquad \frac{\partial U}{\partial F_z^{\text{int}}} = 0, \qquad \frac{\partial U}{\partial M_y^{\text{int}}} = \theta_y, \qquad \frac{\partial U}{\partial M_z^{\text{int}}} = 0. \tag{24}$$

The third expression in Eq. (24) represents the approximate mode-orthogonality condition stated by Eq. (22). One can show that the translational displacement δ_x^{t} is related to the rotation θ_y as

$$\delta_x^{\text{t}} = \frac{d_h\theta_y}{2}. \tag{25}$$

Finally, solving Eqs. (23)–(25) leads to the expression for the rotational spring constant $k_y^{\text{rot}} = M_y^{\text{ext}}/\theta_y$. As pointed out in the introduction, the derivation of k_y^{rot} is given here for the first time.

3.6. Rotational stiffness k_z^{rot} about the z axis

As in the case of k_y^{rot}, the approximate mode-orthogonality of the rotational mode with respect to the translational mode in the y direction is

$$\delta_y^{\text{tip}} = 0. \tag{26}$$

Considering the equilibrium conditions, one can find that

$$F_z^{\text{int}} = 0, \qquad M_x^{\text{int}} = 0, \qquad M_y^{\text{int}} = 0, \tag{27}$$

$$M_z^{\text{ext}} = 4F_x^{\text{int}}\frac{d_v}{2} + 4M_z^{\text{int}}. \tag{28}$$

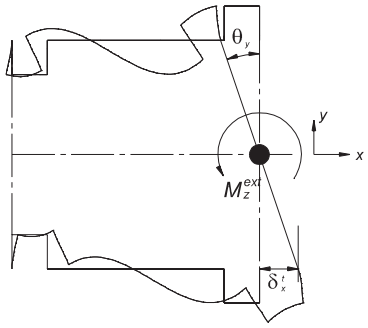

Fig. 9. Deformed shape under M_z^{ext}.

Since the moment about the z axis produces the translational displacement δ_x^{t} as indicated in the Fig. 9, the following kinematic relation must be imposed:

$$\delta_x^{\text{t}} = \frac{d_v \theta_z}{2}. \tag{29}$$

Additional geometric constraints can be imposed from the following relations:

$$\frac{\partial U}{\partial F_x^{\text{int}}} = \delta_x^{\text{t}}, \qquad \frac{\partial U}{\partial F_y^{\text{int}}} = 0, \qquad \frac{\partial U}{\partial M_z^{\text{int}}} = \theta_z. \tag{30}$$

The solution of Eqs. (27)–(30) yields the final expression for k_z^{rot}.

4. Verification of the present analysis

To verify the validity of the present simplified analysis, the present results for the bobbin–suspension system shown in Figs. 2 and 3 are compared with the finite element results. The modeling and analysis is performed by the commercial finite element analysis package, I-DEAS (I-DEAS, 1993). The suspensions are modeled by beam elements and the bobbin is modeled by a concentrated mass.

The values listed in Table 1 are used in the numerical calculation. The thickness and width of the four suspension beams are the same throughout the beams, and are denoted by t_r and b_r, respectively. The suspension beams are assumed to be made of steel (Young's modulus $E = 207$ GPa, shear modulus $G = 79.8$ GPa).

Table 2 compares the results by the present and finite element vibration analyses. Considering the simplifications employed in the present analysis, the present fundamental frequencies are in excellent agreement with those obtained by the detailed finite element analysis. The present analytic solutions may be very useful in situations when a number of calculations are required. In Section 5, we utilize the present analysis for suspension design optimization problems as a practical application example.

Table 1
Numerical values used in the present analysis (units: kg, mm)

h	v	L	b_r	t_r	d_w	d_h	M_c	I_x	I_y	I_z
2.0	1.5	10.0	0.02	0.01	10.0	2.0	0.0023	21.1	26.4	40.1

Table 2
Verification of the first six natural frequencies (unit: Hz)

	Finite element	Present simplified analysis
x translation	175.4	176.2
y translation	14.99	15.08
z translation	17.91	18.46
x rotation	52.48	54.56
y rotation	61.46	59.87
z rotation	302.2	303.0

5. Optimization as an application example

For proper and efficient operations of an optical actuator system, the eigenfrequencies in two major directions of motion must be within a target range, and unwanted higher eigenfrequencies should be made as high as possible. In most practical situations, the rotational vibration mode about the x axis often deteriorates the system performance. Subsequently, the corresponding eigenfrequency needs to be pushed as high as possible. In the present example, the eigenfrequency in the rotational motion about the x axis is chosen as the unwanted eigenfrequency.

The mathematical statement for the present optimization can be stated as

$$\text{minimize}: \quad f(\mathbf{x}) = \frac{1}{k_x^{\text{rot}}}$$

$$\text{subject to}: \quad 24 \leqslant \omega_y^{\text{tr}} \leqslant 26 \text{ Hz}, \quad 24 \leqslant \omega_z^{\text{tr}} \leqslant 26 \text{ Hz},$$

where the design variables $\mathbf{x}$ are $\{h, v, L, b_{\text{AB}}, b_{\text{BC}}, \ldots, b_{\text{GH}}, t_r, d_w, d_h\}^{\text{T}}$.

The constraints impose upper and lower bounds for the fundamental frequencies in the focusing and tracking motions. The design variable b_{ij} $(ij = AB, BC, \ldots, GH)$ denote the width of beam segments (Fig. 3). The thickness of the beam is assumed to be uniform.

The optimization has been conducted using a MATLAB toolbox (Grace, 1996). The optimized design variables and natural frequencies are tabulated in Tables 3, 4, respectively. Table 4 shows some improvements made by the present optimization. Although more practical optimization problems can be handled by the present analysis, this optimization problem is used only to demonstrate the usefulness of the present approach.

Table 3
The numerical values of design variables before and after optimization (unit: mm)

Variables	Before	After
b_{AB}	0.15	0.135
b_{BC}	0.15	0.135
b_{CD}	0.15	0.165
b_{DE}	0.15	0.165
b_{EF}	0.15	0.165
b_{FG}	0.15	0.135
b_{GH}	0.15	0.135
h	2	2.2
v	1.5	1.65
L	10	9.39
t_r	0.15	0.165
d_w	10	11
d_h	4	4.4

Table 4
Values of the natural frequencies before and after optimization (unit: Hz)

	Before	After	Variation (%)
x translation	286.3	258.2	9.84
y translation	24.5	23.4	**4.52**
z translation	24.5	26.0	**6.23**
x rotation	63.6	75.0	**17.9**
y rotation	181.1	181.6	0.25
z rotation	414.7	419.9	1.26

6. Conclusions

Analytic solutions for all six fundamental frequencies of a typical optical actuator are derived for the first time. In particular, the correct deformation shapes and kinematic conditions necessary to determine the rotational modes are offered in this work. Though higher tilting modes and Q-values at some important higher frequencies are not given, the present analysis will play important roles in understanding the mechanics of low-frequency vibration characteristics of pickups and in selecting cost-effective system controllers.

Appendix A. Explicit expressions for strain energy

The strain energy stored in each beam segment can be written as (Fig. 3)

$$U_{\mathrm{AB}} = \int_0^v \frac{(F_x^{\mathrm{int}} y - M_z^{\mathrm{int}})^2}{2EI_{xx}^{\mathrm{AB}}}\mathrm{d}y + \int_0^v \frac{(M_y^{\mathrm{int}})^2}{2GJ^{\mathrm{AB}}}\mathrm{d}y + \int_0^v \frac{(F_z^{\mathrm{int}} y + M_x^{\mathrm{int}})^2}{2EI_{zz}^{\mathrm{AB}}}\mathrm{d}y, \tag{A.1}$$

$$U_{\mathrm{BC}} = \int_0^h \frac{(M_x^{\mathrm{int}} x + F_z^{\mathrm{int}} v)^2}{2GJ^{\mathrm{BC}}}\mathrm{d}x + \int_0^h \frac{(M_y^{\mathrm{int}} - F_z^{\mathrm{int}} x)^2}{2EI_{yy}^{\mathrm{BC}}}\mathrm{d}x + \int_0^h \frac{(F_y^{\mathrm{int}} x - F_x^{\mathrm{int}} v + M_z^{\mathrm{int}})^2}{2EI_{zz}^{\mathrm{BC}}}\mathrm{d}x, \tag{A.2}$$

$$U_{\mathrm{CD}} = \int_0^v \frac{[F_z^{\mathrm{int}}(v-y) + M_x^{\mathrm{int}}]^2}{2EI_{xx}^{\mathrm{CD}}}\mathrm{d}y + \int_0^v \frac{(F_z^{\mathrm{int}} h - M_y^{\mathrm{int}})^2}{2GJ^{\mathrm{CD}}}\mathrm{d}y + \int_0^v \frac{[F_x^{\mathrm{int}}(v-y) - F_y^{\mathrm{int}} h - M_z^{\mathrm{int}}]^2}{2EI_{zz}^{\mathrm{CD}}}\mathrm{d}y, \tag{A.3}$$

$$U_{\mathrm{DE}} = \int_0^L \frac{[M_y^{\mathrm{int}} - F_z^{\mathrm{int}}(h+x)]^2}{2EI_{yy}^{\mathrm{DE}}}\mathrm{d}x + \int_0^L \frac{(M_x^{\mathrm{int}})^2}{2GJ^{\mathrm{DE}}}\mathrm{d}x + \int_0^L \frac{[F_y^{\mathrm{int}}(h+x) + M_z^{\mathrm{int}}]^2}{2EI_{zz}^{\mathrm{DE}}}\mathrm{d}x, \tag{A.4}$$

$$U_{\mathrm{EF}} = \int_0^v \frac{(F_z^{\mathrm{int}} y - M_x^{\mathrm{int}})^2}{2EI_{xx}^{\mathrm{EF}}}\mathrm{d}y + \int_0^v \frac{[F_z^{\mathrm{int}}(h+L) - M_y^{\mathrm{int}}]^2}{2GJ^{\mathrm{EF}}}\mathrm{d}x + \int_0^v \frac{[F_y^{\mathrm{int}}(h+L) + F_x^{\mathrm{int}} y + M_z^{\mathrm{int}}]^2}{2EI_{zz}^{\mathrm{EF}}}\mathrm{d}y, \tag{A.5}$$

$$U_{\mathrm{FG}} = \int_0^h \frac{(F_z^{\mathrm{int}} v - M_x^{\mathrm{int}})^2}{2GJ^{\mathrm{FG}}}\mathrm{d}x + \int_0^h \frac{[M_y^{\mathrm{int}} - F_z^{\mathrm{int}}(L+h+x)]^2}{2EI_{yy}^{\mathrm{FG}}}\mathrm{d}x, \tag{A.6}$$

$$U_{\mathrm{GH}} = \int_0^v \frac{[F_y^{\mathrm{int}}(L+2h) + F_x^{\mathrm{int}}(v-y) + M_z^{\mathrm{int}}]^2}{2EI_{zz}^{\mathrm{GH}}}\mathrm{d}y + \int_0^v \frac{[M_x^{\mathrm{int}} - F_z^{\mathrm{int}}(v-y)]^2}{2EI_{xx}^{\mathrm{GH}}}\mathrm{d}y + \int_0^v \frac{[M_y^{\mathrm{int}} - F_z^{\mathrm{int}}(L+2h)]^2}{2GJ^{\mathrm{GH}}}\mathrm{d}x. \tag{A.7}$$

In Eqs. (A.1)–(A.7), E and G are Young's and shear moduli, respectively. The moments of inertia of the beam segment ij about the k axis and the polar moment of inertia about the centroid of the beam section are denoted by I_{kk}^{ij} and J^{ij}, respectively.

References

Bouwhuis, G., Braat, J., Huijser, A., Pasman, J., van Rosmalen, G., Schouhamer Immknk, K., 1985. Principles of Optical Disc Systems. Adam Hilger, Bristol.

Göpel, W., Hesse, J., Zemel, J.N., 1994. Sensors. VCH, New York.

Grace, A., 1996. MATLAB Optimization Toolbox User's Guide. Mathworks.

I-DEAS, FEM User's Guide. 1993. Structural Dynamics Research Corporation, SDRC, Milford.

Kajiwara, I., Nagamatsu, A., 1993. Optimum design of optical pick-up by elimination of resonance peaks. Journal of Vibration and Acoustics 115 (4), 377–383.

Kim, Y.Y., Kim, J.H., Han, J.Y., 1999. A new optical pick-up suspension design. International Journal of Solid and Structures 36 (17), 2541–2556.

Lee, M.G., Gweon, D.G., Kim, S.M., 1997. Modelling and optimum design of a fine actuator for optical heads. Mechatronics 7 (7), 573–588.

Washizu, K., 1982. Variational Methods in Elasticity and Plasticity, third ed. Pergamon Press, London.

Zheng, Y., 1994. A long load to overnight success. IEEE Spectrum 31, 60–66.